Energy Conversion and Management 214 (2020) 112887

Contents lists available at ScienceDirect

Energy Conversion and Management

journal homepage: www.elsevier.com/locate/enconman

Performance analysis and optimization of an electricity-cooling cogeneration system for waste heat recovery of marine engine

Xiangyang Liu[a], Manh Quang Nguyen[a,b], Maogang He[a,*]

[a] Key Laboratory of Thermal Fluid Science and Engineering of MOE, School of Energy and Power Engineering, Xi'an Jiaotong University, Xi'an 710049, China
[b] Le Quy Don Technical University, Hanoi 122314, Viet Nam

ARTICLE INFO

Keywords:
Rankine cycle
Absorption refrigeration
Waste heat recovery system
Marine engine

ABSTRACT

Recovering the waste heat is meaningful for reducing the fuel consumption and pollution emissions of marine engine (ME). This paper proposes a system to efficiently convert the waste heat of the exhaust gas (EG) and jacket cooling water (JCW) of ME into electrical and cooling energies largely required on the ship. The proposed waste heat recovery system containes three sub-cycles, namely, the steam Rankine cycle (RC), organic Rankine cycle (ORC) and absorption refrigeration cycle (ARC), which perform well in the utilization of high-, medium- and low-temperature heat sources, respectively. The RC is combined with the ORC to recover waste heat from EG. The RC uses a portion of the JCW as a working fluid, while the remaining portion of the JCW is gradually utilized by the ARC and ORC as a driving heat source and a preheating source, respectively. The thermodynamic performance of the proposed waste heat recovery system (WHRS) was evaluated. Furthermore, the effects of the parameters including evaporation pressure, superheat and engine load on WHRS performance were analyzed for design optimization. The designed WHRS can output 7620 kW electricity and 2940 kW cooling energy under the rated operating conditions of the engine which improves the thermal efficiency of the engine by 10.5%, while WHRSs based on single RC and the dual loop ORC can only improve the efficiency by 5.3% and 7.3%, respectively.

1. Introduction

In recent decades, crises related to fossil fuels [1–3] and environmental pollution [4,5] have become serious problems worldwide. Of all the fossil fuel consumed, 60–70% was consumed by internal combustion engine [6]. Marine transportation has a very important position in global trade, and marine engines (MEs) are the largest category of internal combustion engines. Annually, each ME generates a large amount of waste heat per year which is released into the environment along with the exhaust gas (EG), Jacket cooling water (JCW) and scavenge air, etc., which make its thermal conversion efficiency less than 50% [7]. If the waste heat can be partially converted into the energy required on a ship, the fuel consumption and pollution emissions of ME can be reduced, thereby improving the transportation capacity and economic benefits [8–12].

Up to now, significant effort has been made to recover the waste heat of MEs, and to convert it into useful energy using different technologies to meet various needs, such as electrical energy [13–19], cooling capacity [20–22], and seawater desalination [23,24], *etc*. Because of the high demand for electrical energy in marine environments, most attention has been paid to power generation technologies that utilize waste heat. One mature technology is the steam Rankine cycle (RC), which can utilize a high-temperature heat source. In recent years, low-boiling organic working fluids have been used in the Rankine cycle; this is called the organic Rankine cycle (ORC). The ORC has great advantages in low-temperature waste heat recovery compared to the RC [25,26] and is has become a focal point of research [11,27–31]. For example, Cignitti et al. [32] designed a waste heat recovery system (WHRS) based on the ORC for the EG of ME that takes cycle parameters and working fluid into consideration; Yang [33] studied the payback period of the ORC with HFC/HFC or HFC/HFO mixtures as working fluids to recover waste heat from the EG of a large ME.

In addition to electrical energy, the demand for cold storage and air cooling in marine environments is also very high. Absorption refrigeration technology has the advantage of recovering low-grade heat [34–36]. Therefore, many scholars have used the absorption refrigeration cycle (ARC) to convert the waste heat of MEs into cooling capacity. Wang et al. [37] used a double-effect ARC to recover the waste heat from the EG of a ME with a coefficient of performance (COP) of up to 1.1. Xu et al. [38] reviewed studies on the application of ARC in

* Corresponding author.
E-mail address: mghe@mail.xjtu.edu.cn (M. He).

https://doi.org/10.1016/j.enconman.2020.112887
Received 14 February 2020; Received in revised form 20 April 2020; Accepted 21 April 2020
Available online 07 May 2020
0196-8904/

Nomenclature

Abbreviations

WHRS	waste heat recovery system
RC	Steam Rankine cycle
ORC	Organic Rankine cycle
ARC	Absorption refrigeration cycle
ME	Marine engine
COP	Coefficient of performance
EG	Exhaust gas
JCW	Jacket cooling water

Symbols

h	Enthalpy [kJ·kg^{-1}]
s	Entropy [kJ·kg^{-1}·K^{-1}]
m	Mass flow rate [kg·s^{-1}]
p	Pressure [MPa]
W	Mechanical work [kW]
I	Exergy destruction rate [kW]
Q	Quantity of heat [kW]
T	Temperature [K]
η	Efficiency
ε_p	Isentropic efficiency of pump
ε_s	Isentropic efficiency of expander
x	Mass percentage of absorbent and refrigerant

Subscript

a	Absorber
c	Condenser
sup	Superheat
g	Generator
exp	Expander
eva	Evaporator

the waste heat recovery of ME, and indicated that the large amount of heat carried by JCW, scavenge air and lubricant oil also need to be recovered except that of EG. Salmi et al. [39] used the waste heat of the EG, JCW, and scavenge air from the ME to drive an ARC; they found that 70% of the compression electricity could be saved using this system.

Different waste heat recovery technologies have different optimal working temperature ranges. Integrated systems have thus been proposed because they can make better use of waste heat. Liang et al. [40] combined a RC with an ammonia/water ARC to recover the heat from the EG of ME; the designed WHRS can output 5223 kW equivalent electricity under rated conditions. Ouyang et al. [41] instead combined a dual-loop ORC and an ARC to recover heat from the EG of ME.

The RC, ORC and ARC are most suitable for making use of high-, medium- and low- temperature heat, respectively. Compared the combined cycles of RC-ARC and ORC-ARC, RC-ORC-ARC combined cycle can more effectively utilize the waste heat of EG of ME whose temperature close to 573 K. However, no related research has been conducted. Furthermore, previous researches focus on the waste heat of EG, little attention was paid on that of JCW whose temperature is in the range from 343 K to 393 K. ARC cannot completely utilize the heat in JCW because the flow rate of JCW is comparable to that of EG [38,39] and contains a large amount of waste heat. Ship doesn't need so much cooling energy converted from waste heat of JCW.

Therefore, this paper proposes an integrated WHRS based on RC, ORC and ARC to comprehensively convert waste heat in EG and JCW from ME into electrical and cooling energy. RC and ORC are used simultaneously to produce electrical energy. JCW is used for preheating and EG is for evaporation of working fluid in RC and ORC. A part of the cooling water is used as the working fluid of RC, which will not only make a better utilization of waste heat of JCW, but also results in lower ship weight compared with the method using extra fresh water. An ARC is used to recover the heat of from the rest of the JCW. The thermodynamic performance of the designed system is simulated and analyzed for optimization design.

2. System description

2.1. Waste heat sources of marine engine

The ME that was selected for the present study is that of the MAN B &W 14K98ME-C7.1-TII containership; the output power of the engine at rated conditions is 84280 kW [42]. There are two main waste heat sources, EG and JCW, that are valuable for recovery; their main characteristics under different conditions are presented in Table 1 [42]. The temperature of the JCW at the engine outlet was set to 358 K, and the temperature of the EG from the engine changed with the engine load.

2.2. Waste heat recovery system

The WHRS designed in this study is shown in Fig. 1. The temperature-entropy diagram is shown in Fig. 2. It uses the RC, ORC, and ARC to recover the aste heat of the EG and JCW from the ME. When the engine is working, the WHRS can simultaneously generate electrical energy and cooling energy. First, a portion of the JCW from the engine is pressurized by a pump to the working pressure. It then enters heat exchanger 1 and becomes steam after absorbing heat from the EG. Subsequently, there is a large drop in the temperature of the EG, but it still contains a large amount of heat that can be recovered. Thus, the EG is used as the heat source for an ORC, transforming the working fluid to a superheated gas. The steam enters expander 1 to generate mechanical work and is condensed into a liquid state in condensor 1. Then, water returned to the engine to cool the engine cylinders again.

The RC requires a portion of the JCW as the circulating working fluid; the remaining JCW is used as the heat source for the generator in the ARC, as shown in Fig. 1. In the ARC, the JCW heats the solution in the generator, and the refrigerant is desorbed. The refrigerant is then condensed into liquid in condenser 4, and its pressure is reduced by a throttle. Subsequently, the refrigerant enters the evaporator to absorb heat and realize refrigeration. It is then absorbed by the absorbent in

Table 1
The mass flow rate and temperature of the exhaust gas.

Engine load (%)	Engine power (kW)	Mass flow rate of JCW (kg·s^{-1})	Mass flow rate of EG (kg·s^{-1})	Temperature of EG (K)
110	92,708	196.3	223.4	560.6
100	84,280	181.8	202.0	557.2
95	80,066	174.4	191.3	555.7
90	75,852	166.9	180.6	554.2
85	71,638	159.4	170.1	552.4
80	67,424	151.8	159.5	550.5
75	63,210	144.1	148.9	548.3
70	58,996	136.3	138.4	546.4
65	54,782	128.4	127.9	544.2
60	50,568	120.3	117.5	541.8
55	46,354	112.2	107.1	539.5
50	42,140	103.9	96.9	536.4
45	37,926	95.4	86.6	532.8
40	33,712	86.8	76.4	530.0
35	29,498	77.9	66.2	526.4
30	25,284	68.8	56.1	521.3

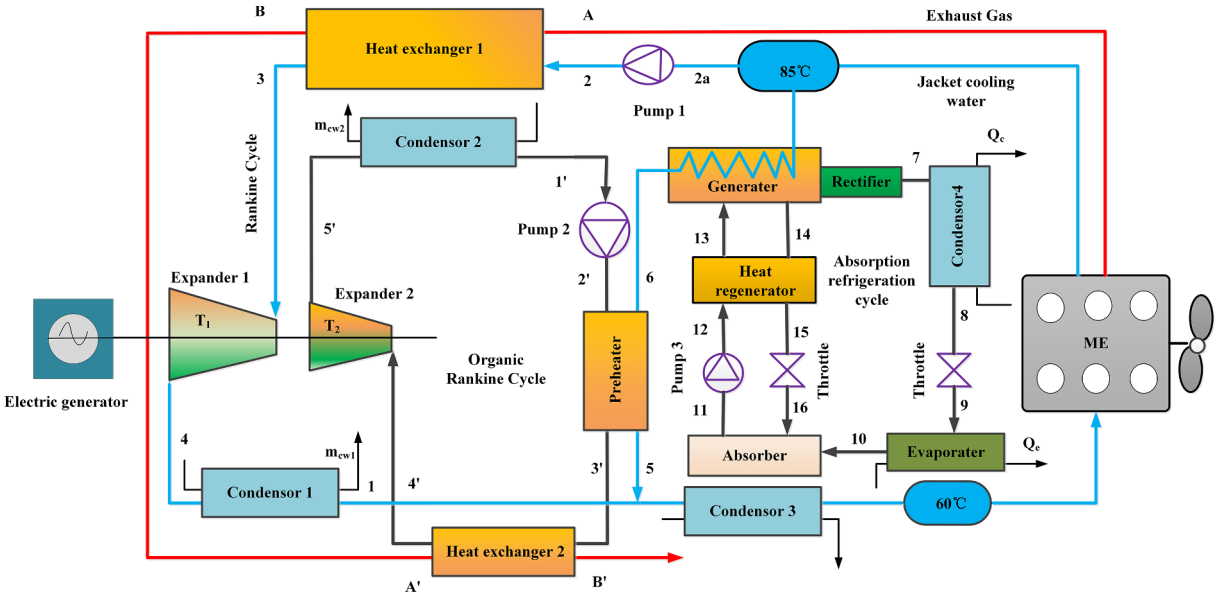

Fig. 1. Schematic diagram of waste heat recovery system for marine engine.

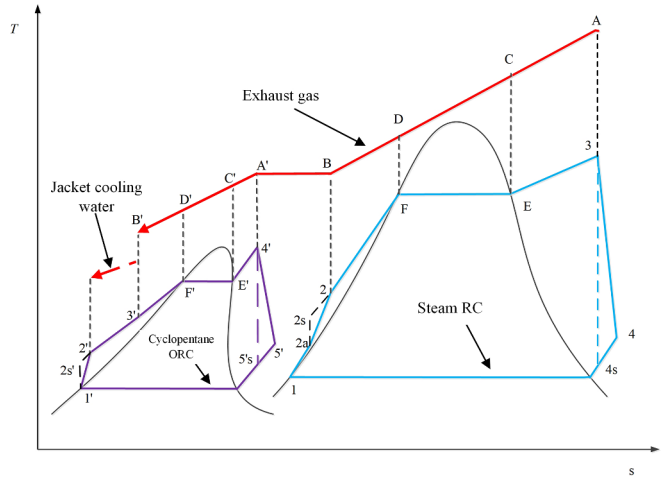

Fig. 2. T-S diagram for RC and ORC sub-cycle.

the absorber, which forms a strong solution. The strong solution is sent to the generator by a solution pump. After the refrigerant is desorbed, the strong solution becomes a weak solution. The weak solution heats the strong solution in the heat regenerator and then enters the absorber after its pressure is reduced by a throttle.

In the ORC, the working fluid is pressurized by pump 2 and then preheated by the JCW. This is to recover more heat from the JCW, which still has a high temperature of about 353 K. After that, the working fluid in the ORC enters heat exchanger 2 to absorb the high-temperature heat of the EG; it becomes gas and then expands to generate mechanical work in expander 2. After expansion, the working fluid is cooled in condenser 2 and becomes liquid. Finally, the working fluid returns to the liquid pump to complete a closed cycle.

The discharge temperature of the EG ($T_{B'}$) is set to be not lower than 413 K in this work because if it is lower than the acid dew point (393–403 K), it will corrode the equipment. The temperature of the JCW returning to the engine should not be too low; otherwise, the combustion efficiency of the engine will be reduced. Thus, the JCW sent back to the engine is selected to be no less than 333 K.

3. Mathematical model

As described above, the WHRS in this work includes three sub-cycles: the RC, ARC, and ORC. In order to analyse the performance of the WHRS, thermodynamic models for the three sub-cycles were established based on the law of conservation of energy and the law of conservation of mass. Simulations were carried out using MATLAB software.

3.1. Thermodynamic model for RC

The RC is used to recover high-grade heat from the EG and consists of pump 1, heat exchanger 1, expander 1, and condenser 1. The thermodynamic model established for the RC refers to references [43,44]. The mass flow rate (m_w) of water in the RC is calculated by Eqs. (1) and (2) as follows:

$$T_D = T_F + \Delta T_m \tag{1}$$

$$m_w = \frac{m_g c_{pg}(T_A - T_D)}{h_3 - h_F} \tag{2}$$

where T_A, T_D, and T_F are the temperatures at points A, D, and F, respectively; ΔT_m is the pinch point temperature; m_g is the mass flow rate of the EG; c_{pg} is the specific heat capacity of the EG; and h_3 and h_F are the enthalpies of water at points 3 and F, respectively. The consumed power (W_p) and exergy destruction rate (I_p) of pump 1 for the pressurization of water in the RC are given by

$$W_p = m_w(h_2 - h_{2a}) = \frac{m_w(h_{2s} - h_{2a})}{\varepsilon_p} \tag{3}$$

$$I_p = m_w T_0(s_2 - s_{2a}) \tag{4}$$

where h_2 and h_{2a} are the enthalpies of water after and before, respectively, being compressed by pump 1; h_{2s} is the enthalpy of water in isentropic compression (calculated by REFPROP 9.1) [45]; s_2 and s_{2a} are the entropies of water after and before, respectively, being compressed by pump 1; ε_p is the isentropic efficiency of pump 1; and T_0 is the ambient temperature. During heat exchange processes 2 to 3 in heat exchanger 1, the EG discharges heat and its temperature decreases, while the water absorbs heat and its temperature rises. The heat exchange capacity (Q_{he1}) and the destroyed exergy rate (I_{he1}) in heat exchanger 1 are given by

$$Q_{he1} = m_w(h_3 - h_2) = m_g c_{pg}(T_A - T_B) \quad (5)$$

$$I_{he1} = Q_{he1}\left(1 - \frac{T_0}{T_{ave}}\right) + m_w(h_2 - h_3 - T_0(s_2 - s_3)) \quad (6)$$

$$T_{ave} = \left(\frac{T_A - T_B}{\ln\frac{T_A}{T_B}}\right) \quad (7)$$

where T_{ave} is the average temperature of EG in heat exchanger 1 and h_3 and s_3 are the enthalpy and entropy of the water at point 3, respectively.

The mechanical work output (W_{exp1}) and exergy destruction rate (I_{exp1}) in expander 1 are given by

$$W_{exp\,1} = m_w(h_3 - h_4) = m_w\varepsilon_s(h_{4s} - h_3) \quad (8)$$

$$I_{exp\,1} = m_w T_0(s_4 - s_3) \quad (9)$$

where s_4 and h_4 are the entropy and enthalpy of water at point 4, respectively; ε_s is the isentropic efficiency of expander 1; and h_{4s} is the enthalpy of water in the isentropic expansion process (calculated by REFPROP 9.1 [45]).

The heat released from the water steam during condensation processes 4 to 1 in condenser 1 (Q_{c1}) is calculated by

$$Q_{c1} = m_w(h_4 - h_1) \quad (10)$$

where h_1 is the enthalpy of water at point 1. The flow of cooling water m_{cw1} in the condenser 1 is:

$$m_{cw1} = \frac{Q_{c1}}{(h_{w1,in} - h_{w1,out})} \quad (11)$$

Where $h_{w1,\,out}$ and $h_{w1,\,in}$ are the enthalpies of cooling water at outlet and inlet of the condenser 1, respectively.

The exergy destruction rate of the condensation process in condenser 1, I_{c1} is calculated as follows

$$I_{c1} = m_w(h_4 - h_1 - T_0(s_4 - s_1)) + m_{cw1}(h_{w1,in} - h_{w1,out} - T_0(s_{w1,in} - s_{w1,out})) \quad (12)$$

where $s_{w1,\,out}$ and $s_{w1,\,in}$ are the entropies of cooling water at outlet and inlet of the condenser 1, respectively.

The mechanical work output W_{RC} and exergy destruction rate I_{RC} of RC are given by

$$W_{RC} = W_{exp\,1} - W_P \quad (13)$$

$$I_{RC} = I_P + I_{he1} + I_{exp1} + I_{c1} \quad (14)$$

The thermal efficiency (η_{RC}) and the exergy efficiency (η'_{RC}) of RC are given by

$$\eta_{RC} = \frac{W_{RC}}{Q_{he1}} \quad (15)$$

$$\eta'_{RC} = \frac{W_{RC}}{W_{RC} + I_{RC}} \quad (16)$$

3.2. Thermodynamic model for ARC

In this work, the ARC is used to recover the waste heat of the JCW from the ME and to produce cooling energy, as shown in Fig. 1. It consists of several main components: a generator, condenser, evaporator, absorber, pump, and heat regenerator. In this work, NH_3/H_2O and H_2O/LiBr were tested as the working pair of the ARC. When NH_3/H_2O is used, the ARC needs a rectifier because NH_3 and H_2O have a relatively small difference between their boiling points; therefore, both NH_3 and H_2O exist in the vapour phase in the generator. The thermophysical properties of refrigerants can be obtained from REFPROP 9.1. The basic mass balance and energy balance in the generator of the ARC are expressed as [46,47]

Table 2
Parameters of the WHRS.

Properties	Value	Units
Isentropic efficiency of pump	0.8	
Pinch point temperature in heat exchanger 1	20	K
Pinch point temperature in heat exchanger 2	8	K
Isentropic efficiency of expander	0.8	
Initial temperature of cooling water	25	K
Pinch point temperature in condenser	5	K
Discharge temperature of EG	413	K
Efficiency of electric generator	0.96	
Pinch point temperature in generator	5	K
Efficiency of heat regenerator	0.8	
Ambient temperature	298	K

Table 3
The coefficients in Eq. (22d) [49,50].

i	m_i	n_i	a_i	i	m_i	n_i	a_i
1	0	1	−7.6108	9	2	1	2.84179×10^0
2	0	4	2.56905×10^1	10	3	3	7.41609×10^0
3	0	8	-2.47092×10^2	11	5	3	8.91844×10^2
4	0	9	3.25952×10^2	12	5	4	-1.61309×10^3
5	0	12	-1.58854×10^2	13	5	5	6.22106×10^2
6	0	14	6.19084×10^1	14	6	2	-2.07588×10^2
7	1	0	1.14314×10^1	15	6	4	-6.87393×10^0
8	1	1	1.18157×10^0	16	8	0	3.50716×10^0

Table 4
The constants in Eq. (23c) [51].

n	a_n	b_n	c_n	d_n
0	−954.8	-3.293×10^{-1}	7.428×10^{-3}	-2.269×10^{-6}
1	47.77	4.076×10^{-2}	-1.514×10^{-4}	
2	−1.592	-1.361×10^{-5}	1.355×10^{-6}	
3	2.094×10^{-2}	-7.136×10^{-6}		
4	-7.689×10^{-5}			

$$m_{13} = m_{14} + m_7 \quad (17)$$

$$m_{13}h_{13} = m_{14}h_{14} + m_7h_7 \quad (18)$$

$$m_{13}x_{13} = m_{14}x_{14} + m_7 \quad (19)$$

where m_{13} and x_{13} are the mass flow rate of the weak solution and the mass percentage of the refrigerant in the weak solution, respectively; m_{14} and x_{14} are the mass flow rate of the strong solution and the mass percentage of the refrigerant in the strong solution, respectively; m_7 and h_7 are the mass flow rate and enthalpy of the refrigerant, respectively; and h_{13} and h_{14} are the enthalpies of the strong solution and weak solution, respectively. The following equations are used to calculate m_{13} and m_{14}:

$$m_{13} = \frac{1 - x_{14}}{x_{13} - x_{14}}m_7 \quad (20)$$

$$m_{14} = \frac{1 - x_{13}}{x_{13} - x_{14}}m_7 \quad (21)$$

The saturation pressure of the NH_3/H_2O mixture can be calculated as a function of temperature [48,49]

$$\lg P/\text{kPa} = A - \frac{B}{T/K} \quad (22a)$$

where

$$A = 7.44 - 1.767x + 0.9823x^2 + 0.3627x^3 \quad (22b)$$

$$B = 2013.8 - 2155.7x + 1540.9x^2 - 194.7x^3 \quad (22c)$$

The enthalpy of the NH_3/H_2O mixture can be calculated based on

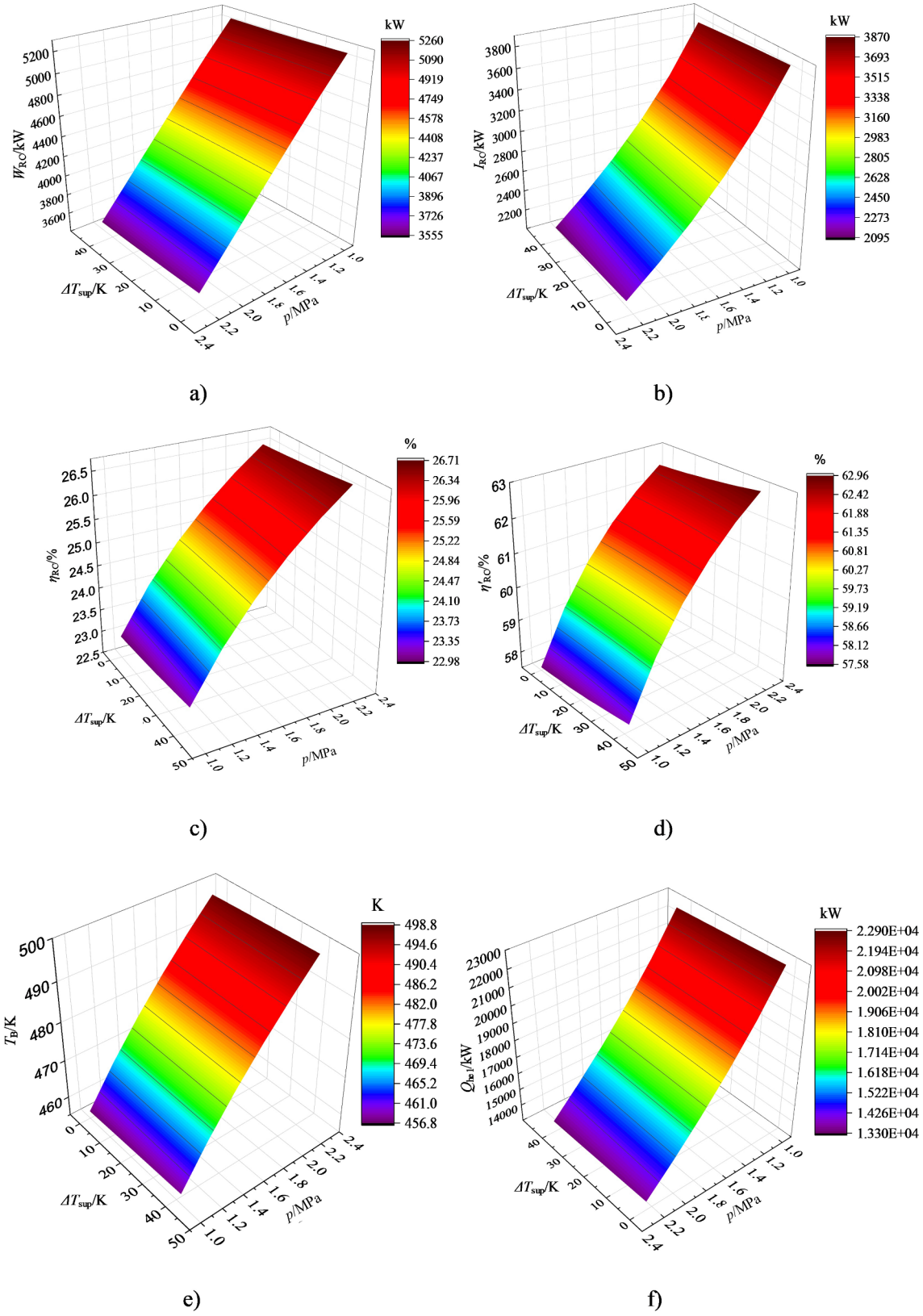

Fig. 3. Effect of evaporation pressure and superheat of RC on its performance.

the temperature and concentration as follows:

$$h(T,\bar{x}) = 100\sum_{i=1}^{16} a_i \left(\frac{T}{273.16} - 1\right)^{m_i} \bar{x}^{n_i} \tag{22d}$$

where a_i, m_i and n_i (i = 1–16) are coefficients which are given in Table 3, $\bar{x}$is given by

$$\bar{x} = \frac{17.03x}{17.03x + 18.015(1-x)} \tag{22e}$$

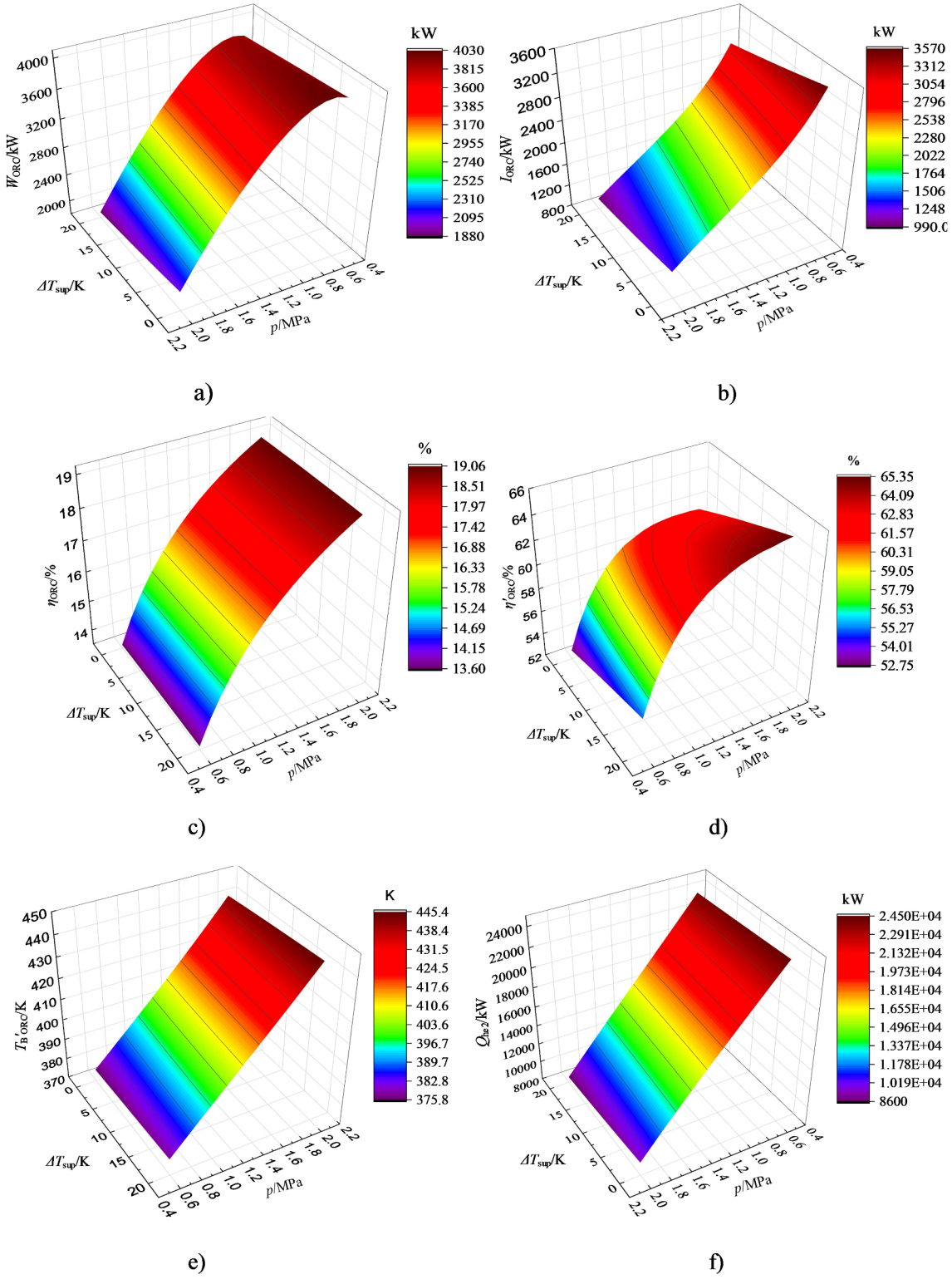

Fig. 4. Effect of evaporation pressure and superheat of ORC on its performance.

The concentrations of the strong and weak H_2O/LiBr solutions can be calculated from the temperatures in the condenser, evaporator, absorber, and generator [50]:

$$X_s = \frac{49.04 + 1.125T_g - T_c}{134.65 + 0.47T_g} \tag{23a}$$

$$X_w = \frac{49.04 + 1.125T_a - T_{eva}}{134.65 + 0.47T_a} \tag{23b}$$

where X_s and X_w are the concentrations of LiBr (kg LiBr/kg solution) in the strong and weak solutions, respectively, and T_g, T_c, T_a, and T_{eva} are the temperatures in K in the generator, condenser, absorber, and evaporator, respectively.

The enthalpy of the H_2O/LiBr solution is calculated by [51]

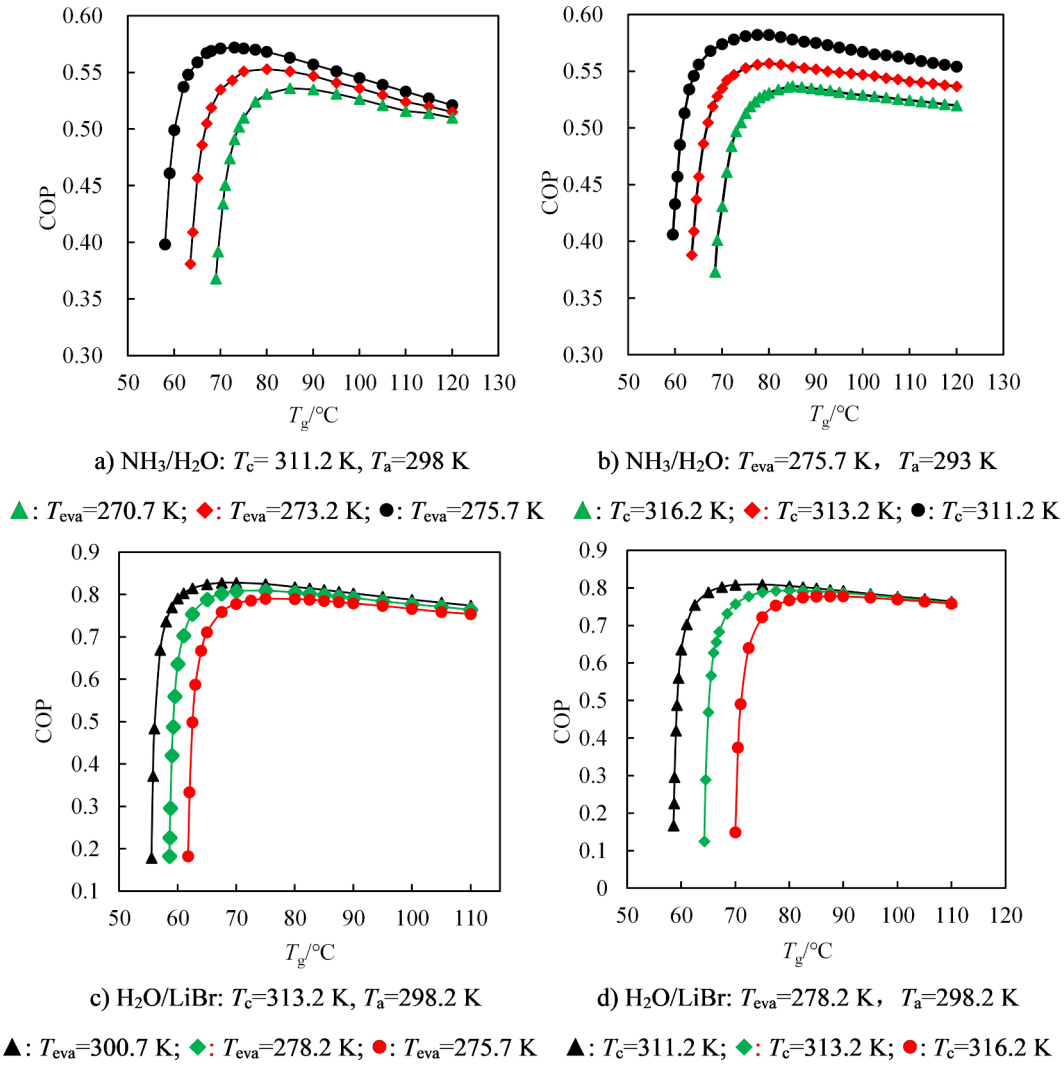

Fig. 5. Effect of T_g, T_a, T_c, and T_{eva} on the performance of ARC.

$$h(T,X) = \sum_{j=0}^{4} a_j X^j + T\sum_{j=0}^{3} b_j X^j + T^2\sum_{j=0}^{2} c_j X^j + T^3 d_0 \tag{23c}$$

where T is the temperature of the solution, which is between 273 K and 463 K; X is the concentration of the absorbent in the solution (kg LiBr/kg solution); and a_n, b_n, c_n, and d_n are parameters whose values are given in Table 4.

The energy balance in the heat regenerator is described as

$$T_{15} = \varepsilon T_{11} + (1-\varepsilon)T_{14} \tag{24}$$

$$m_{14}(h_{14} - h_{15}) = m_{13}(h_{13} - h_{12}) \tag{25}$$

where h_{15} and h_{12} are the enthalpies of the solution at points 15 and 12, respectively; ε is the efficiency of the heat regenerator. The power consumed by pump 3 (W_{p3}) is calculated by

$$W_{p3} = m_{13}(h_{12} - h_{11}) \tag{26}$$

where h_{11} is the enthalpy of the solution at point 11. Knowing the requirements of cooling energy, the mass flow rate of the refrigerant in the evaporator is defined by the energy conservation law as follows:

$$m_7 = m_9 = \frac{Q_e}{h_{10} - h_9} \tag{27}$$

where h_9 and h_{10} are the enthalpies of the solution at points 9 and 10, respectively, and Q_e is the cooling capacity of the evaporator. Given all of the enthalpies and mass flow rates, the energy changes in the generator (Q_{ge}), absorber (Q_a), and condenser (Q_c) can be calculated by

$$Q_{ge} = m_7 h_7 + m_{14} h_{14} - m_{13} h_{13} \tag{28}$$

$$Q_a = m_{10} h_{10} + m_{16} h_{16} - m_{11} h_{11} \tag{29}$$

$$Q_c = m_7(h_8 - h_7) \tag{30}$$

where h_{16} and m_{16} are the enthalpy and mass flow rate of the solution at point 16, respectively; m_7 is the mass flow rate of the refrigerant at point 7; and m_{10} and m_{11} are the mass flow rates of the solution at points 10 and 11, respectively. If the thermoelectric conversion efficiency is 0.38, the coefficient of performance (*COP*) is defined as

$$COP = \frac{Q_e}{Q_{ge} + \frac{W_{p3}}{0.38}} \tag{31}$$

3.3. Thermodynamic model for ORC

The mass flow rate of the organic working fluid (m_f) can be calculated by

$$m_f = \frac{m_g c_{p_g}(T_{A'} - T_{D'})}{h_{4'} - h_{F'}} \tag{32a}$$

$$T_{D'} = \Delta T_{m'} + T_{F'} \tag{32b}$$

where $T_{A'}$, $T_{D'}$, and $T_{F'}$ are the temperatures at points A′, D′ and F′,

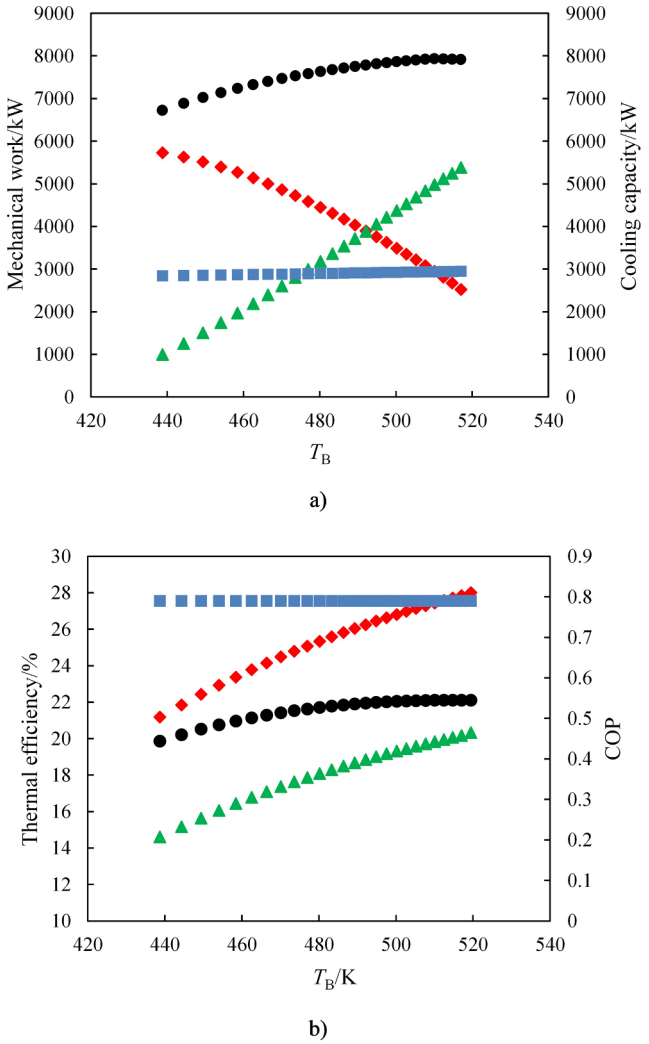

Fig. 6. Effect of T_B on the performance of WHRS and its sub-cycles. ▲: ORC; ◆: RC; ●: WHRS; ■:ARC.

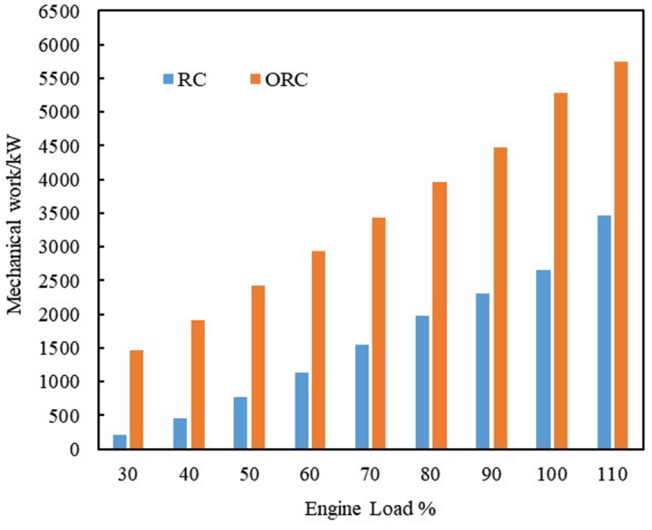

Fig. 7. Contribution of RC and ORC for output mechanical work.

respectively; $\Delta T_{m'}$ is the pinch point temperature; and $h_{4'}$ and $h_{F'}$ are the enthalpies of the organic working fluid at points 4′ and F′, respectively.

The inlet temperature of the EG at heat exchanger 2 is equal to the outlet temperature of heat exchanger 1:

$$T_{A'} = T_B = T_D - m_w \frac{h_F - h_2}{m_g c_{pg}} \tag{33}$$

The temperature of the EG at point B′ ($T_{B'}$) can be obtained by the following equation:

$$T_{B'} = T_{D'} - \frac{m_f (h_{3'} - h_{2'})}{m_g c_{pg}} \tag{34}$$

The consumed power (W_{p2}) and exergy destruction rate (I_{p2}) of pump 2 are given by the following equations:

$$W_{p2} = m_f (h_{2'} - h_{1'}) = m_f \frac{h_{2s'} - h_{1'}}{\varepsilon_p} \tag{35}$$

$$I_{p2} = m_f T_0 (s_{2'} - s_{1'}) \tag{36}$$

where $h_{1'}$ and $h_{2'}$ are the enthalpies of the organic working fluid at points 1′ and 2′, respectively; $h_{2s'}$ is the enthalpy of the organic working fluid in isentropic compression (calculated by REFPROP 9.1); and $s_{1'}$ and $s_{2'}$ are the entropies of the organic working fluid at points 1′ and 2′, respectively. During processes $\hat{2}$ to $\hat{3}$ in the preheater, the heat of the JCW is recovered to preheat the working fluid. The heat exchange (Q_{ph}) and exergy destruction rate (I_{ph}) in the preheater are calculated by the following equations:

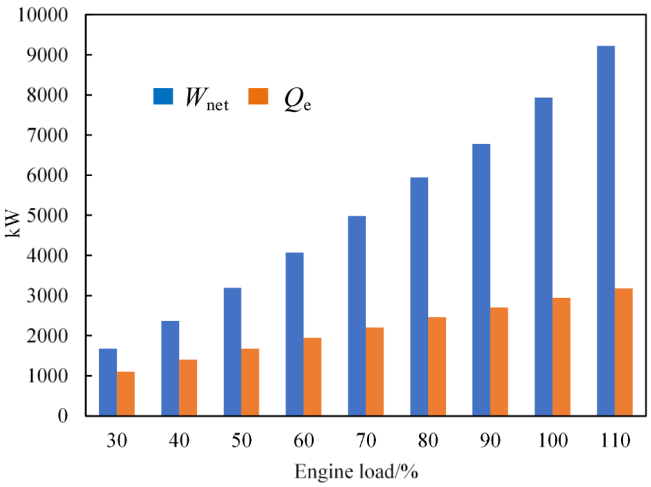

Fig. 8. Total output mechanical work and cooling capacity of the designed WHRS.

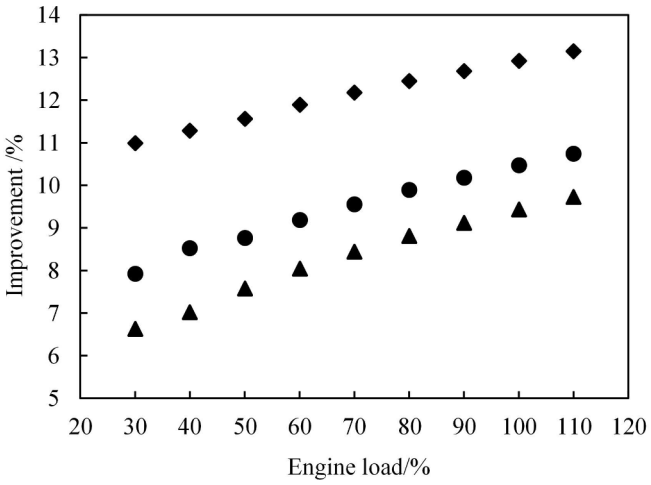

Fig. 9. The improvement in the performance of the engine. ◆, η_{IOC}; ●, η_{EIMW}; ▲, η_P.

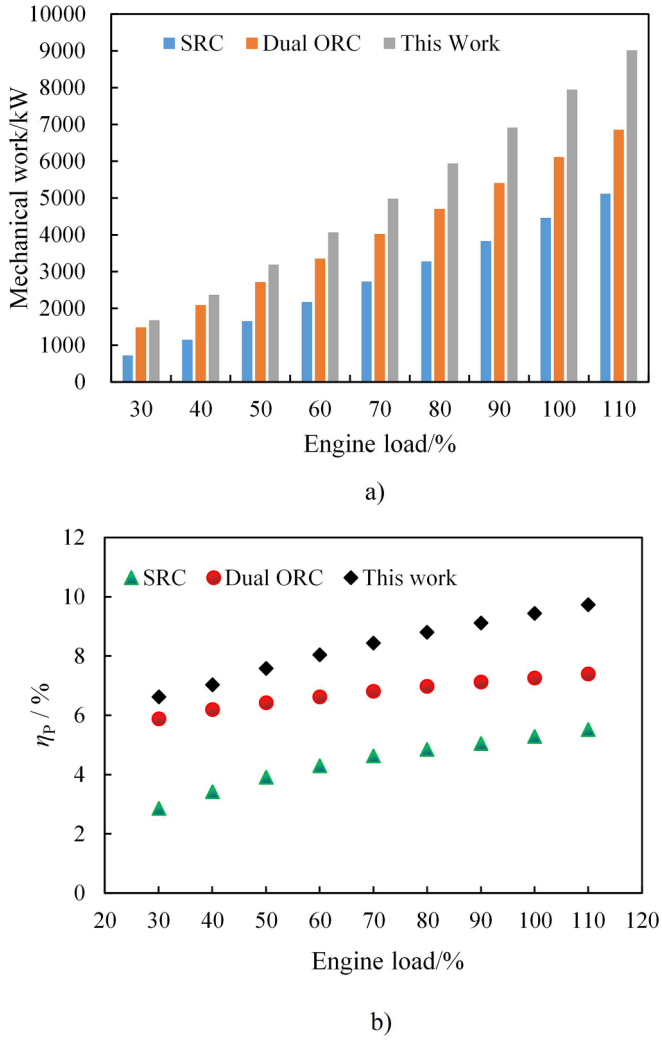

Fig. 10. Comparison of the WHRS proposed in this work to the SRC and dual-loop ORC systems.

$$Q_{ph} = m_f(h_{3'} - h_{2'}) = m_6(h_6 - h_5) \tag{37}$$

$$I_{ph} = m_6(h_6 - h_5 - T_0(s_6 - s_5)) + m_f(h_{2'} - h_{3'} - T_0(s_{2'} - s_{3'})) \tag{38}$$

where $h_{3'}$ and $s_{3'}$ are the enthalpy and entropy of the organic working fluid at point 3′, respectively; h_6 and h_5 are the enthalpies of the JCW at points 6 and 5, respectively; and s_6 and s_5 are the entropies of the JCW at points 6 and 5, respectively.

The heat exchange (Q_{he2}) and exergy destruction rate (I_{he2}) in heat exchanger 2 are expressed as

$$Q_{he2} = m_f(h_{4'} - h_{3'}) = m_g c_{pg}(T_{A'} - T_{B'}) \tag{39}$$

$$I_{he2} = Q_{he2}\left(1 - \frac{T_0}{T_{ave'}}\right) + m_f(h_{3'} - h_{4'} - T_0(s_{3'} - s_{4'})) \tag{40}$$

$$T'_{ave} = \left(\frac{T_{A'} - T_{B'}}{\ln\frac{T_{A'}}{T_{B'}}}\right) \tag{41}$$

where T'_{ave} is the average temperature of EG in heat exchanger 2.

The mechanical work output (W_{exp2}) and exergy destruction rate (I_{exp2}) in expander 2 are calculated by

$$W_{exp2} = m_f(h_{4'} - h_{5'}) = m_f\varepsilon_s\left(h_{4'} - h_{5s'}\right) \tag{42}$$

$$I_{exp2} = m_f T_0(s_{5'} - s_{4'}) \tag{43}$$

where $s_{4'}$ and $h_{4'}$ are the entropy and enthalpy of the organic working fluid at point 4′, respectively; $s_{5'}$ and $h_{5'}$ are the entropy and enthalpy of the organic working fluid at point 5′, respectively; and h_{5s} is the enthalpy of the organic working fluid in the isentropic expansion process (calculated by REFPROP 9.1 [45]).

The amount of heat exchanged in condenser 2 is expressed as

$$Q_{c2} = m_f(h_{5'} - h_{1'}) \tag{44}$$

The flow of cooling water (m_{cw2}) in condenser 2 is

$$m_{cw2} = \frac{Q_{c2}}{h_{w2,out} - h_{w2,in}} \tag{45}$$

where $h_{w2,\ out}$ and $h_{w2,\ in}$ are the enthalpies of the cooling water at the outlet and inlet of condenser 2, respectively.

The exergy destruction rate in condenser 2 (I_{c2}) is calculated as follows:

$$I_{c2} = m_f(h_{5'} - h_{1'} - T_0(s_{5'} - s_{1'}) + m_{cw2}(h_{w2,in} - h_{w2,out} - T_0(s_{w2,in} - s_{w2,out}) \tag{46}$$

where $s_{w2,\ out}$ and $s_{w2,\ in}$ are the entropies of the cooling water at the outlet and inlet of condenser 2, respectively.

The mechanical work output (W_{ORC}) and exergy destruction rate (I_{ORC}) of the ORC are calculated by

$$W_{ORC} = W_{exp\,2} - W_{p2} \tag{47}$$

$$I_{ORC} = I_{p2} + I_{ph} + I_{he2} + I_{c2} + I_{exp\,2} \tag{48}$$

The thermal efficiency (η_{RC}) and exergy efficiency (η'_{RC}) of the ORC are given by

$$\eta_{ORC} = \frac{W_{ORC}}{Q_{ph} + Q_{he2}} \tag{49}$$

$$\eta'_{ORC} = \frac{W_{ORC}}{I_{ORC} + W_{ORC}} \tag{50}$$

3.4. Thermal and exergy efficiency of the waste heat recovery system

The total mechanical work output of the whole system (W_{net}) includes the work from the RC and ORC, which can be expressed as

$$W_{net} = W_{RC} + W_{ORC} \tag{51}$$

The thermal efficiency of the designed WHRS (η_t) is calculated by

$$\eta_t = \frac{W_{net} + Q_e}{Q_{ge} + Q_{he1} + Q_{he2} + Q_{ph}} \tag{52a}$$

The output work efficiency of the designed WHRS (η_{net}) is calculated by

$$\eta_{net} = \frac{W_{net}}{Q_{he1} + Q_{he2} + Q_{ph}} \tag{52b}$$

The exergy efficiency of the output work in the designed WHRS (η_E) is calculated by

$$\eta_E = \frac{W_{net}}{W_{net} + I_{in}} \tag{53}$$

where $I_{in} = I_{RC} + I_{ORC}$ is the total exergy destruction rate of the designed WHRS.

3.5. Calculation conditions

Before calculating the thermodynamic performance of the designed WHRS, some parameters need to be set. Their values are provided in Table 2. The selection of organic working fluids directly affects the performance of an ORC [52–54]. Therefore, many scholars have studied the performance of working fluids in ORCs [55–58]. According to the design conditions of this study, cyclopentane was selected as the

working fluid, as recommended in the literature [59].

4. Results and discussion

4.1. Thermodynamic analysis of RC and ORC

RC and ORC are used to cascade utilize the heat of exhaust gas and produce electrical power. Fig. 3 shows the effects of evaporation pressure (p) and superheat (ΔT_{sup}) of RC on its performance. It can be seen that the higher the evaporation pressure is, the smaller the output mechanical work as shown in Fig. 3a. The reason is that the higher the evaporation pressure is, the higher the evaporation temperature which results in an increase in the temperature of exhaust gas at the outlet of heat exchanger 1 as shown in the Fig. 3e. Further, it results in less heat of the EG being recovered by RC as shown in Fig. 3f. On the contrary, the thermal efficiency of RC has an increasing trend as shown in Fig. 3c. In addition, as evaporation pressure rises, the exergy destruction rate decreases, and the exergy efficiency increases as shown in Fig. 3b and d. Compared with the evaporation pressure, the effect of superheat of RC on its output work, exergy destruction rate, thermal efficiency and exergy efficiency and the recovered heat of exhaust gas is slight. The reason is that as the superheat of RC increases, the enthalpy of steam at point 3 only has slight change, which results in a slight change in the heat input into the RC and the temperature difference in heat exchanger 1.

Fig. 4 shows the effects of superheat and evaporation pressure of the ORC on its performance with $T_{A'}$ at 483 K. Because the superheat and evaporation pressure of ORC has no effect on RC and ARC, therefore the effects of superheat and evaporation pressure of ORC on its performance is same to that on WHRS. Generally, as the superheat and evaporation pressure increase, the output mechanical work and exergy destruction rate of the ORC decrease, as shown in Fig. 4a and b, respectively, whereas the thermal efficiency and exergy efficiency exhibit a contrary tendency, as shown in Fig. 4c and d, respectively. Compared with RC, the effect of the superheat of the ORC is more pronounced. According to the results provided in Fig. 4e and f, it can be concluded that the smaller the superheat and evaporation pressure are, the lower the released temperature and the more heat can be recovered from the exhaust gas.

4.2. Thermodynamic analysis of ARC

There are four factors that have an important influence on the performance of the ARC: generation temperature (T_g), absorption temperature (T_a), condensation temperature (T_c), and evaporation temperature (T_{eva}). Fig. 5 shows the effects of these four factors on ARC performance with NH_3/H_2O (Fig. 5a and b) or H_2O/LiBr (Fig. 5c and d) as the working pair. It can be observed that the COP of the ARC changes monotonically with T_a, T_c, and T_{eva}: the COP increases as T_{eva} increases and decreases as T_c or T_a increases. In contrast, as T_g increases, the COP first increases and then decreases. As expected, H_2O/LiBr produces a higher COP than NH_3/H_2O. At $T_{eva} = 275.7$ K and $T_a = 298$ K, the COP of H_2O/LiBr reaches 0.79, which is much higher than that of NH_3/H_2O (0.57), although the T_c for H_2O/LiBr is higher than that for NH_3/H_2O, but NH_3/H_2O has a much lower T_{eva}.

4.3. Thermodynamic analysis of WHRS

The effects of the parameters of the ORC and ARC on the performance of the whole WHRS are the same as the effects on the ORC and ARC themselves because the ORC and ARC have no influence on the other sub-cycles. The evaporation pressure and superheat of the RC have a significant influence on the performance of the total mechanical work output of the WHRS. The evaporation pressure and the superheat of RC determine the temperature of exhaust gas for heating the working fluid of RC and ORC; meanwhile, they also affect the amount of JCW, which is the heat source of the ARC. When the temperature of the exhaust gas remains unchanged, the effects of the evaporation pressure and superheat of RC are reflected in the effects of T_B which is the combined temperature point of the RC and ORC sub-cycles. Therefore, Fig. 6 shows the effect of T_B on the performance of each sub-cycle and the whole WHRS at the engine load of 100% and the optimal condition. T_a, T_c and T_{eva} are set to 298 K, 313.2 K and 278.2 K, respectively while the superheat of RC and ORC is set to 20 K and 10 K, respectively. It can be seen that the larger the T_B, the smaller output mechanical work of RC, but the greater the total output mechanical work as shown in Fig. 6a. For thermal efficiency, ORC and RC both show rising trends, but the output work efficiency of the WHRS first increases with increasing of T_B and reaches the highest value $\eta_{net} = 22\%$, and then slowly declines as shown in Fig. 6b. Since the flow rate of water in RC decreases as T_B rises, the flow rate of JCW for providing heat for the generator in ARC increases, so the cooling energy also gradually increases. The COP of ARC is unchanged because the heat source temperature does not change.

In order to clearly show the contributions of the two sub-cycles, RC and ORC, at different engine loads, the output mechanical work of the RC and ORC at the optimal condition is shown in Fig. 7. The superheat of RC and ORC is set to 20 K and 10 K, respectively. It can be observed that the ORC accounts for a larger proportion of the output mechanical work than the RC does and that the contribution of the ORC to the output mechanical work increases with the decreasing engine load. Our system is therefore better than a single RC or ORC. In addition, as can be seen from Fig. 8, the output mechanical work and the cooling capacity of the proposed WHRS increase as the engine load rises, reaching 7938 kW (which can produce 7620 kW of electricity if the efficiency of mechanical work converted into electricity is 0.96) and 2940 kW, respectively, under rated conditions (100%).

If the ME works 300 days per year at an engine load of 100%, the electricity saved by the designed WHRS over one year is

$$A = 0.96 \times A_{work} + \frac{A_{cooling}}{COP_c} = 60.91 \times 10^6 \text{ (kWh)} \tag{54}$$

where COP_c is the COP of the compression refrigeration system used in the current ship. In this work, the COP_c was taken as 3.5. Based on a fuel combustion efficiency of 176 g·kWh^{-1}, the designed WHRS can save 10,720 tons of fuel per year.

Three factors were defined to evaluate the performance of the designed WHRS. The first is the improvement in the output capability, - which is defined as

$$\eta_{IOC} = \frac{W_{net} + Q_e}{P_e} \tag{55}$$

where P_e is the engine power. The second is the improvement in the mechanical output of the engine, which is defined as

$$\eta_P = \frac{W_{net}}{P_e} \tag{56}$$

The third is the equivalent improvement in the mechanical work output of the engine, which is defined as

$$\eta_{EIMW} = \frac{W_{net} + \frac{Q_e}{0.96 \times COP_c}}{P_e} \tag{57}$$

Fig. 9 shows η_{IOC}, η_{EIMW}, and η_P under different engine loads. Obviously, the designed WHRS significantly improves the performance of the studied engine. When the engine load is 100%, η_P, η_{EIMW}, and η_{IOC} are 9.4%, 10.5%, and 12.9%, respectively. Currently, it is common to use a WHRS based on a single RC to recover the waste heat of MEs. Therefore, the proposed WHRS was compared with a WHRS design based on a single RC (SRC) in Fig. 10. To verify the advantage of the proposed WHRS, it was also compared with the dual-loop ORC system proposed by Song and Gu [60] in Fig. 10. The results show that the

output mechanical work and the improvement in the mechanical output (η_P) of the engine from the proposed WHRS are approximately 78% and 30% greater than those from the SRC and dual-loop ORC systems under the rated conditions of the engine, while the equivalent improvement in the mechanical work output from the proposed WHRS is 98% and 44% greater than for those from the SRC and the dual loop ORC system, respectively.

5. Conclusion

In this study, an integrated WHRS was designed for utilization of the waste heat from ME to produce the electricity and cooling energy. Based on the above analysis, the WHRS designed in this study has the following characteristics:

1) The proposed WHRS based on the RC, ORC and ARC can not only make a highly efficient utilization of the waste heat from the EG and JCW which are at different grades because the sub-cycles of the RC, ORC and ARC are excellent for recovering high-, medium- and low-temperature heat, respectively, but also product the electrical and cooling energy flexibly to meet the demand on the ship.
2) The evaporation pressure and superheat of the RC and ORC determine their output mechanical work, while the temperatures in the generator, absorber, condenser, and evaporator determine the cooling capacity of the ARC. Reasonable optimization of the combined temperature (T_B) of the two sub-cycles (RC and ORC) can effectively improve the total output mechanical work of the WHRS. In addition, as the engine load increases, the output power and cooling capacity of the designed WHRS both increase.
3) The designed WHRS significantly improves the thermodynamic performance of the ME. When applied to the MAN B&W 14K98ME-C7.1-TII ME, 7938 kW output power and 2940 kW cooling capacity can be achieved by the designed WHRS under 100% engine load of 82480 kW. Correspondingly, the designed WHRS can save 10,720 tons of fuel per year.

CRediT authorship contribution statement

Xiangyang Liu: Conceptualization, Methodology, Writing - review & editing. **Manh Quang Nguyen:** Software, Data curation, Writing - original draft. **Maogang He:** Supervision, Funding acquisition, Writing - review & editing.

Declaration of Competing Interest

The authors declare that they have no known competing financial interests or personal relationships that could have appeared to influence the work reported in this paper.

Acknowledgments

The supports for the present work provided by the National Natural Science Foundation of China (No. 51525604 and No. 51721004), China Postdoctoral Science Foundation (No. 2019T120906) and Overseas Expertise Introduction Project for Discipline Innovation (No. B16038) are gratefully acknowledged.

References

[1] Hu J, Liu C, Li Q, et al. Molecular simulation of thermal energy storage of mixed CO2/IRMOF-1 nanoparticle nanofluid. Int J Heat Mass Transf 2018;125:1345–8.
[2] Liu X, Lan T, Wang C, Nguyen M, Zhang Y, He M. Measurement of critical temperature and critical pressure of tert-butanol and alkane mixtures. J Mol Liq 2020;112582.
[3] Liu X, Zhu C, Yang F, Su C, He M. Experimental and correlational study of isobaric molar heat capacities of fatty acid esters: ethyl nonanoate and ethyl dodecanoate. Fluid Phase Equilib 2019;479:47–51.
[4] Armellini A, Daniotti S, Pinamonti P, Reini M. Reducing the environmental impact of large cruise ships by the adoption of complex cogenerative/trigenerative energy systems. Energy Convers Manage 2019;198:111806.
[5] Liu X, He M, Lv N, Xu H, Bai L. Selective absorption of CO2 from H2, O2 and N2 by 1-hexyl-3-methylimidazolium tris (pentafluoroethyl) trifluorophosphate. J Chem Thermodyn 2016;97:48–54.
[6] Yang MH. Optimizations of the waste heat recovery system for a large marine diesel engine based on transcritical Rankine cycle. Energy 2016;113:1109–24.
[7] Shu G, Liu L, Tian H, et al. Parametric and working fluid analysis of a dual-loop organic Rankine cycle (DORC) used in engine waste heat recovery. Appl Energy 2014;113:1188–98.
[8] Kyriakidis Fotis, et al. Modeling and optimization of integrated exhaust gas re-circulation and multi-stage waste heat recovery in marine engines. Energy Convers Manage 2017;151:286–95.
[9] Nawi ZM, Kamarudin SK, Abdullah SRS, et al. The potential of exhaust waste heat recovery (WHR) from marine diesel engines via organic rankine cycle. Energy 2019;166:17–31.
[10] Chatzopoulou MA, Markides CN. Thermodynamic optimisation of a high-electrical efficiency integrated internal combustion engine–organic Rankine cycle combined heat and power system. Appl Energy 2018;226:1229–51.
[11] Mondejar ME, Andreasen JG, Pierobon L, et al. A review of the use of organic Rankine cycle power systems for maritime applications. Renew Sustain Energy Rev 2018;91:126–51.
[12] Yuan H, Sun P, Zhang J, et al. Theoretical and experimental investigation of an absorption refrigeration and pre-desalination system for marine engine exhaust gas heat recovery. Appl Therm Eng 2019;150:224–36.
[13] Zhang H, Guan X, Ding Y, et al. Emergy analysis of Organic Rankine Cycle (ORC) for waste heat power generation. J Cleaner Prod 2018;183:1207–15.
[14] Meroni A, Andreasen JG, Persico G, et al. Optimization of organic Rankine cycle power systems considering multistage axial turbine design. Appl Energy 2018;209:339–54.
[15] Daghigh R, Shafieian A. An investigation of heat recovery of submarine diesel engines for combined cooling, heating and power systems. Energy Convers Manage 2016;108:50–9.
[16] Braimakis K, Karellas S. Energetic optimization of regenerative Organic Rankine Cycle (ORC) configurations. Energy Convers Manage 2018;159:353–70.
[17] Bahrampoury R, Behbahaninia A. Thermodynamic optimization and thermo-economic analysis of four double pressure Kalina cycles driven from Kalina cycle system. Energy Convers Manage 2017;152:110–23.
[18] Hoang AT. Waste heat recovery from diesel engines based on Organic Rankine Cycle. Appl Energy 2018;231:138–66.
[19] Chen H, Goswami DY, Rahman MM, et al. A supercritical Rankine cycle using zeotropic mixture working fluids for the conversion of low-grade heat into power. Energy 2011;36(1):549–55.
[20] Yang S, Deng C, Liu Z. Optimal design and analysis of a cascade LiBr/H_2O absorption refrigeration/ transcritical CO_2 process for low-grade waste heat recovery. Energy Convers Manage 2019;192:232–42.
[21] Moreno D, Ferro VR, de Riva J, et al. Absorption refrigeration cycles based on ionic liquids: refrigerant/absorbent selection by thermodynamic and process analysis. Appl Energy 2018;213:179–94.
[22] Mohammadi A, Kasaeian A, Pourfayaz F, et al. Thermodynamic analysis of a combined gas turbine, ORC cycle and absorption refrigeration for a CCHP system. Appl Therm Eng 2017;111:397–406.
[23] Borsani R, Rebagliati S. Fundamentals and costing of MSF desalination plants and comparison with other technologies. Desalination 2005;182(1–3):29–37.
[24] Elshorbagy W, Abdulkarim M. Chlorination byproducts in drinking water produced from thermal desalination in United Arab Emirates. Environ Monit Assess 2006;123(1–3):313–31.
[25] Li J, Duan Y, Yang Z, et al. Exergy analysis of novel dual-pressure evaporation organic Rankine cycle using zeotropic mixtures. Energy Convers Manage 2019;195:760–9.
[26] Eyerer S, Dawo F, Kaindl J, et al. Experimental investigation of modern ORC working fluids R1224yd (Z) and R1233zd (E) as replacements for R245fa. Appl Energy 2019;240:946–63.
[27] Yu G, Shu G, Tian H, et al. Experimental investigations on a cascaded steam-/organic-Rankine-cycle (RC/ORC) system for waste heat recovery (WHR) from diesel engine. Energy Convers Manage 2016;129:43–51.
[28] Liu X, Wang T, He M. Investigation on the condensation process of HFO refrigerants by molecular dynamics simulation. J Mol Liq 2019;288:111034.
[29] Sun J, Liu Q, Duan Y. Effects of evaporator pinch point temperature difference on thermo-economic performance of geothermal organic Rankine cycle systems. Geothermics 2018;75:249–58.
[30] Shi L, Shu G, Tian H, et al. A review of modified Organic Rankine cycles (ORCs) for internal combustion engine waste heat recovery (ICE-WHR). Renew Sustain Energy Rev 2018;92:95–110.
[31] Mahmoudi A, Fazli M, Morad MR. A recent review of waste heat recovery by Organic Rankine Cycle. Appl Therm Eng 2018;143:660–75.
[32] Cignitti S, Andreasen JG, Haglind F, et al. Integrated working fluid-thermodynamic cycle design of organic Rankine cycle power systems for waste heat recovery. Appl Energy 2017;203:442–53.
[33] Yang Min-Hsiung. Payback period investigation of the organic Rankine cycle with mixed working fluids to recover waste heat from the exhaust gas of a large marine diesel engine. Energy Convers Manage 2018;162:189–202.
[34] Aly WIA, Abdo M, Bedair G, et al. Thermal performance of a diffusion absorption refrigeration system driven by waste heat from diesel engine exhaust gases. Appl Therm Eng 2017;114:621–30.

[35] Liu X, Ye Z, Bai L, et al. Performance comparison of two absorption-compression hybrid refrigeration systems using R1234yf/ionic liquid as working pair. Energy Convers Manage 2018;181:319–30.
[36] Liu X, Nguyen MQ, Xue S, et al. Vapor-liquid equilibria and inter-diffusion coefficients for working pairs for absorption refrigeration systems composed of [HMIM][BF4] and fluorinated propanes. Int J Refrig 2019;104:34–41.
[37] Wang M, Becker TM, Schouten BA. Ammonia/ionic liquid based double-effect vapor absorption refrigeration cycles driven by waste heat for cooling in fishing vessels. Energy Convers Manage 2018;174:824–43.
[38] Xu X, Li Y, Yang SY, et al. A review of fishing vessel refrigeration systems driven by exhaust heat from engines. Appl Energy 2017;203:657–76.
[39] Salmi W, Vanttola J, Elg M, et al. Using waste heat of ship as energy source for an absorption refrigeration system. Appl Therm Eng 2017;115:501–16.
[40] Liang Y, Shu G, Tian H, et al. Investigation of a cascade waste heat recovery system based on coupling of steam Rankine cycle and NH_3-H_2O absorption refrigeration cycle. Energy Convers Manage 2018;166:697–703.
[41] Ouyang T, Su Z, Huang G, et al. Modeling and optimization of a combined cooling, cascaded power and exhaust gas purification system in marine diesel engines. Energy Convers Manage 2019;200:112102.
[42] MAN B&W K98ME-C7.1-TII. Project Guide Electronically Controlled Two stroke Engines. 2014; https://marine.man-es.com/applications/projectguides/2stroke/content/printed/K98ME-C7_1.pdf.
[43] Choi BC, Kim YM. Thermodynamic analysis of a dual loop heat recovery system with trilateral cycle applied to exhaust gases of internal combustion engine for propulsion of the 6800 TEU container ship. Energy 2013;58:404–16.
[44] Fu J, Liu J, Ren C, et al. An open steam power cycle used for IC engine exhaust gases energy recovery. Energy 2012;44(1):544–54.
[45] Lemmon EW, Huber ML, McLinden MO. NIST standard reference database 23, reference fluid thermodynamic and transport properties (REFPROP), Version 9.1, National Institute of Standards and Technology, Gaithersburg MD; 2013.
[46] Ouadha A, Elgotni Y. Integration of an ammonia-water absorption refrigeration system with a marine diesel engine: a thermodynamic study. Procedia Comput Sci 2013;19:754–61.
[47] Kumar V, Pandya B, Patel J, et al. Cut-off temperature evaluation and performance comparison from energetic and exergetic perspective for NH_3-H_2O absorption refrigeration system. Therm Sci Eng Progr 2017;4:97–105.
[48] Sun DW. Comparison of the performances of NH_3-H_2O, NH_3-$LiNO_3$ and NH_3-NaSCN absorption refrigeration systems. Energy Convers Manage 1998;39:357–68.
[49] Bourseau P, Bugarel R. Absorption-diffusion machines: comparison of the performances of NH_3/H_2O and NH_3/NaSCN. Int J Refrig 1986;9(4):206–14.
[50] Lansing FL. Computer modeling of a single stage lithium bromide/water absorption refrigeration unit. Jet Propulsion Laboratory, California Institute of Technology, Pasadena, CA, Deep Space Network Progress Report 1976;42:247–57.
[51] Kaita Y. Thermodynamic properties of lithium bromide–water solutions at high temperatures. Int J Refrig 2001;24:374–90.
[52] Li J, Liu Q, Ge Z, et al. Thermodynamic performance analyses and optimization of subcritical and transcritical organic Rankine cycles using R1234ze (E) for 100–200° C heat sources. Energy Convers Manage 2017;149:140–54.
[53] Chen Q, Xu J, Chen H. A new design method for Organic Rankine Cycles with constraint of inlet and outlet heat carrier fluid temperatures coupling with the heat source. Appl Energy 2017;98:562–73.
[54] Xu J, Yu C. Critical temperature criterion for selection of working fluids for subcritical pressure Organic Rankine cycles. Energy 2014;74:719–33.
[55] Ge Z, Li J, Liu Q, et al. Thermodynamic analysis of dual-loop organic Rankine cycle using zeotropic mixtures for internal combustion engine waste heat recovery. Energy Convers Manage 2018;166:201–14.
[56] Chang H, Wan Z, Zheng Y, et al. Energy-and exergy-based working fluid selection and performance analysis of a high-temperature PEMFC-based micro combined cooling heating and power system. Appl Energy 2017;204:446–58.
[57] Preißinger M, Schwöbel JAH, Klamt A, et al. Multi-criteria evaluation of several million working fluids for waste heat recovery by means of Organic Rankine Cycle in passenger cars and heavy-duty trucks. Appl Energy 2017;206:887–99.
[58] Scaccabarozzi R, Tavano M, Invernizzi CM, et al. Comparison of working fluids and cycle optimization for heat recovery ORCs from large internal combustion engines. Energy 2018;158:396–416.
[59] He MG, Zhang XX, Zeng K, Gao K. A combined thermodynamic cycle used for waste heat recovery of internal combustion engine. Energy 2011;36:6821–9.
[60] Song J. Gu C Parametric analysis of a dual loop Organic Rankine Cycle (ORC) system for engine waste heat recovery. Energy Convers Manage 2015;105:995–1005.